Laser Pulses Characterization with Pyroelectric Sensors

9

Laser Pulses Characterization with Pyroelectric Sensors

Lorenzo Capineri[1] and Marina Mazzoni[2]
[1]*Dipartimento Elettronica e Telecomunicazioni,*
Università di Firenze
[2]*IFAC CNR*
Italy

1. Introduction

There are many industrial and medical applications of CO_2 (λ=10.6 μm) and Nd:YAG (λ=1.06 μm) infrared lasers for which the quality of the process are tightly connected to the characteristic of the laser pulse. These two types of lasers deliver pulses with duration, repetition frequency and power that can be controlled by means of a programmable electronic control unit. An open-loop control generally optimize the process performances by availing of a laser system model. However, this method cannot control that during the operation the laser source and the optical delivering system could deteriorate; moreover the laser beam characteristics and laser pulse temporal envelope could change by several factors like power supply variations, optical beam misalignments, dirty deposits on mirrors, changes in laser efficiency and many others .
For these reasons it is of crucial importance to provide array of sensors capable to measure both the laser pulse and beam characteristics on-line. These sensors generally require the design of front-end electronics for signal conditioning , processing and visualization at a rate equal to the laser pulse repetition frequency.
This chapter illustrates the capabilities offered by pyroelectric arrays of sensors for this aim. The main advantage of the pyroelectric thermal sensors is an extended spectral response beyond 100μm that includes the CO_2 gas infrared lasers.and the quantum cascade (QC) lasers. Chemical sensing at room temperature with pulsed QC-DFB lasers operating at 15.6 μm has been developed (Kosterev et al., 2002); in this paper also a spatial distribution of the laser power was made with a pyroelectric sensor, as in other spectroscopic applications which employed infrared lasers (Toci G. et al., 2000). This type of sensors can be fabricated with low-cost pyroelectric materials. The simulated time and frequency responses are particularly useful for their design which in turn must be tailored for the reproducibility characterization of the laser pulses. The sensor signals depend on the adopted fabrication, packaging technology, and on and the gain-to-frequency factor of the front-end electronics beside the pyroelectric material properties. A limited bandwidth, sensitivity and linearity *vs* power density generate distortions of the output signal. Consequently, the designer has to consider a certain amount of distortion of the laser pulse that must evaluated for a proper monitoring operation and eventually minimized. The analysis of this type of distortions is fundamental to optimize the design of pyroelectric sensors. Moreover, the front-end electronics can include the filtering

(analog or digital) of the signals to compensate distortions. Among the several ferroelectric materials, in this chapter we focus on PVDF (polynivilidene – fluoride) array of sensors.
The chapter illustrates examples of the applications of these sensors, which were derived from academic research projects in collaboration with companies. It will be shown how to use, design and built monitoring systems for mid infrared (IR) laser pulses. Moreover, we provide the basic assemblying principles of pyroelectric transducers and front-end electronics for a quick and easy reproduction by professionals involved in laser pulse monitoring and laser processes optimization.

2. Pyroelectric sensors modelling

The use of CO_2 power lasers systems for industrial (welding, marking, etc.) and medical (surgery and therapy, etc.) applications are now numerous and of increasing importance. These systems necessitate of low-cost detectors able to measure the laser beam characteristics for process optimisation. Pyroelectric sensors are the most suitable devices for the measurement of industrial lasers characteristics (power and energy) because of their broad spectral response and ruggedness. The pyroelectric detectors can be conveniently utilized for the radiation detection by high power (> 1 kW) CO_2 continuous wave (CW) lasers, by means of mechanical chopper for the detected radiation modulation necessary for their operation. With the recent generation of CO_2 pulsed lasers, which can achieve pulse repetition frequency higher than 100 Hz, a temperature gradient on the sensor can be used in place of the mechanical modulation. This section is aimed to describe the design a pyroelectric sensor with response optimised for high-power CO_2 laser applications for which the requirement of a short settling time is much more stringent than voltage responsitivity.
Pyroelectric sensors based on PVDF polymer foils are suitable for designing detectors, in the mid mid IR region, with response time sufficiently fast for monitoring and controlling CO_2 lasers at high pulse repetition frequency (PRF >100Hz). In the following we describe how to design and built single and multi-element detectors, capable of following the laser pulses evolution with rising times of about 0.05 ms and about 2 ms (FWHM) duration. For monitoring these lasers pulses it is necessary to provide sensors with sufficient short time response to follow these rapid rising edges.
The choice of PVDF pyroelectric materials offers the possibility to produce low cost, large area detectors which can be installed inside the laser system or close to the target under laser processing. These detectors, assembled in a matrix array configuration can be also used for real-time control of the laser beam profile.

2.1 Materials and methods

Pyroelectric detectors have been designed by using a theoretical sensor model with multilayer structure (Setiadi & Regtien, 1995). The computational results reported are relative to the configuration shown in Figure 1, where the multilayer structure is composed by a pyroelectric film, a bonding layer and a substrate. The heat sink at the top at the bottom of the structure is represented by the air surrounding the sensor.
An equivalent circuit of a multylayer sensor can be obatined, see Figure 2, where the thermal and electrical characteristics can be represented by resistive-capacitive impedances.
The pyroelectric current $I(t)$ results proportional to the time derivative of the excess mean temperature of the pyroelectric layer. For a sinusoidal incident power density $P_s(t) = P_i e^{j\omega t}$ at angular frequency ω, the current responsivity in the frequency domain results in the following expression:

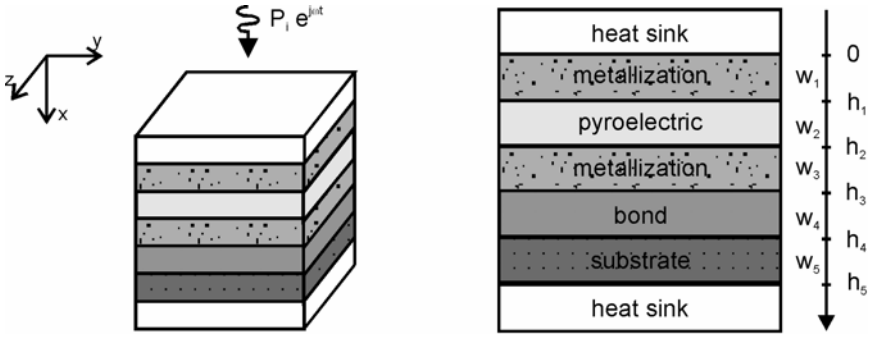

Fig. 1. Multilayer model of a pyroelectric detector; w_i is the thickness of layer i , A is the active area of the sensor exposed to a modulated incident radiation $P_s(t) = P_i e^{(j\omega t)}$ along the x direction

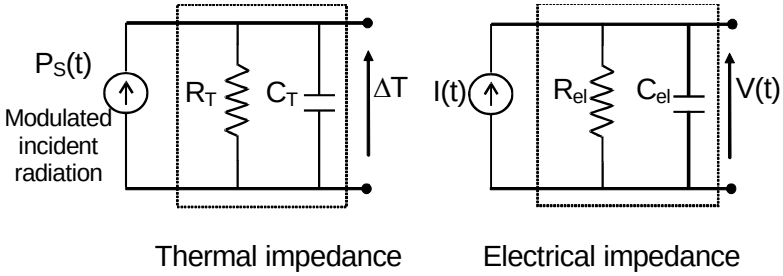

Fig. 2. Pyroelectric sensor equivalent circuit.

$$I(\omega) = \frac{j\omega Ap\eta P_i}{w_p \alpha_p} \cdot \left[A_p(\exp(w_p\alpha_p) - 1)) + B_p(1 - \exp(-w_p\alpha_p)) \right] \quad (1)$$

where η is the absorbance, p is the pyroelectric coefficient, *A* the sensor active surface; w_p and α_p are the thickness and the reciprocal of the thermal diffusion distance of the pyroelectric layer, respectively. For a structure of the sensor with N layers, the coefficients A_p and B_p are derived from the steady-state solutions of a linear system of N equations (Setiadi & Regtien, 1995).

The current responsivity optimization can be analyzed as a function of the different physical parameters of the multilayer structure. Figure 3 and Figure 4 show the frequency responses of a typical detector as a function of the thicknesses of the PVDF film and of the metallization, respectively. These last two parameters revealed the most significant in the design optimization. The results which we show refer to an active area of the sensor of A=1cm², and a pyroelectric coefficient of λp=20μC/ m²K. The measurements were performed at a power density of 1 mW/mm². The values of the materials properties deduced from literature (Giacoletto and Landee et. al., 1977)(Regtien et. al., 1992) are reported in Table 1.

The current amplitude generated by a given incident power density can be estimated by means of simulations involving Equation (1). For the values reported previously, the current amplitude varies from nA to tens μA in the frequency range 1Hz-100kHz. These pyroelectric current values require a front-end electronic design with precision, low bias-current operational amplifiers.

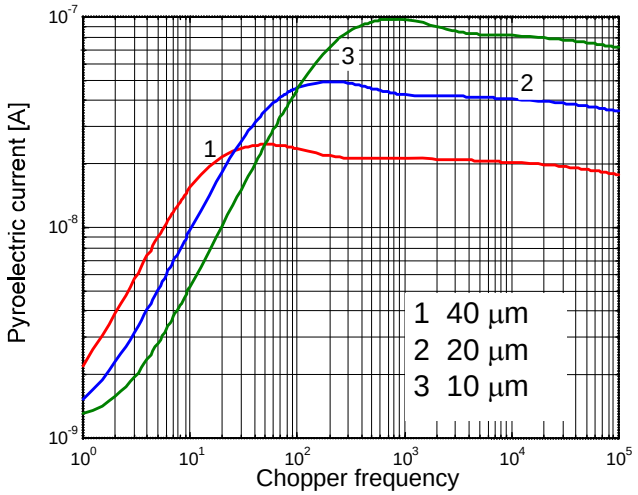

Fig. 3. Pyroelectric current responsivities for different thicknesses of the PVDF layer.

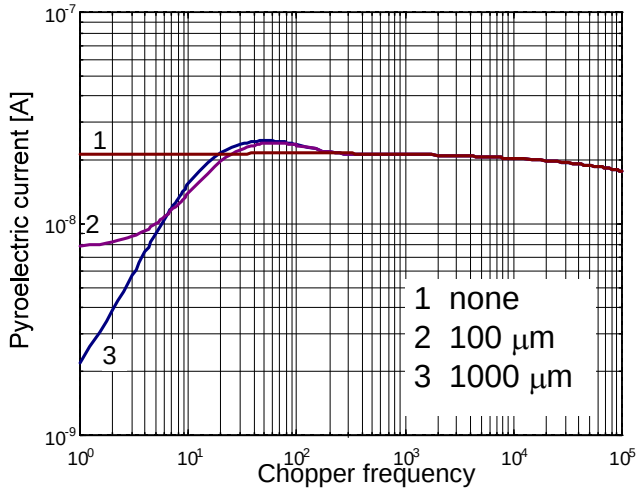

Fig. 4. Pyroelectric current responsivities for different thicknesses of the copper substrate.

When sensors are built in a matrix array, the thermal cross-talk between adjacent elements must also be evaluated. and the lateral heat conduction (Schopf et al.,1989), which was omitted in (1), must be taken into account in the simulations. To account for the lateral heat conduction along the direction y (and similarly for direction z), a basic relationship is reported:

$$T(y,t) = T_b \cdot e^{-\frac{y}{\lambda_D}} \cdot e^{j\left(\omega \cdot t - \frac{y}{\lambda_D}\right)} \tag{2}$$

where T_b is the temperature at the boundary of a pixel and $\omega=2\pi f_{chop.}$ The thermal cross-talk results reported in Figure 5 for different values of chopper frequency (f_{chop}), were obtained with the following parameters: pixel area=200μm x 200 μm, $\lambda_D=(2D/2\pi f_{chop})^{0.5}$ penetration depth, D=0.0056 cm^2/s temperature diffusivity.The results shown in Figure 5 point out the advantage of working with a high pulse repetition rate (>100 Hz) in the industrial and medical laser applications that require arrays of sensors.

Layer	Material	Thermal conductivity [W/cm K]	Thermal capacitance [J/cm³ K]	Thickness [μm]
Metallization	Gold	3.10	2.83	0.07
Pyroelectric	PVDF	0.0013	2.30	40
				20
				10
Metallization	Gold	3.10	2.83	0.07
Bonding		1	1.65	1
Substrate	Silicon	1.49	1.64	1000
				100
				0

Table 1. Physical parameters used in the simulations shown in Figures 3 and 4.

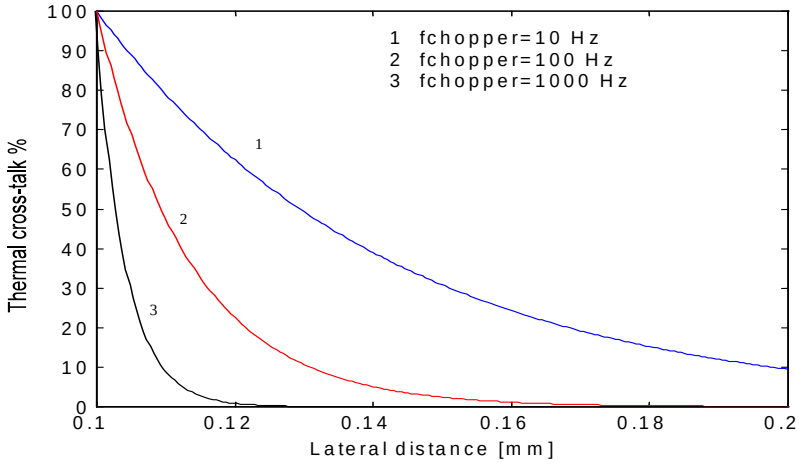

Fig. 5. Thermal cross-talk between two elements (area 0.2x0.2 mm^2 each) as function of the lateral distance from boundary (y=0).

The designed front-end electronics is based on a low-noise transimpedance amplifier in order to convert the current generated by the detector in a voltage signal with signal-to-noise ratio suitable for a successive analog or digital signal processing. In Table 2, Z_{el} is the feedback impedance formed by the parallel circuit R_a and C_c of the basic configuration of the transimpedance amplifier shown in Figure 6. It can be easily demonstrated that, for an ideal

operational amplifier, the voltage response can be written as Vo=Ip * Z_{el} , and the -3dB cut-off frequency as $f_{cut\text{-}off} = 1 / 2\pi R_a C_c$. According to the values shown in Table 2, the cut-off frequency resulted 10.6 kHz.

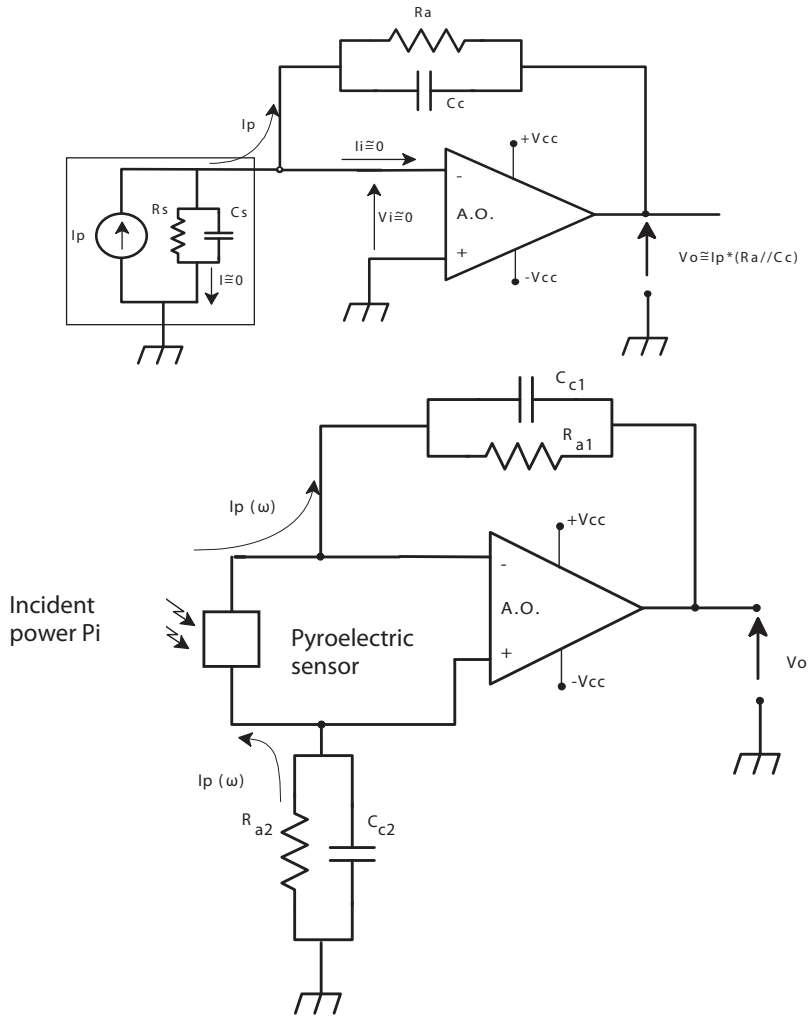

Fig. 6. Top) Basic transimpedance amplifier for a pyrolectric transducer with single ended (unbalanced) connetion; Bottom) Differential (balanced) configuration of transimpedance amplifier with $R_{a1}= R_{a2}$ and $C_{a1}= C_{a2}$. The differential configuration has a gain twice the single ended configuration and improved common mode noise rejection.

The usefulness of sensor and preamplifier modeling with electronic CAD programs is the possibility of calculating the current or voltage responsivity function for a given shape of the laser pulse. According to this approach (Capineri et al. , 2000), a temporal and frequency analysis of arbitrary modulated laser intensity have been demonstrated possible. The

experimental detector pulse time response of 24 μs to a simulated 17 μs rising edge of a Nd-YAG laser pulse is shown in Figure 7. By a fitting process based on the root mean square error the model parameters can be retrieved with good accuracy .

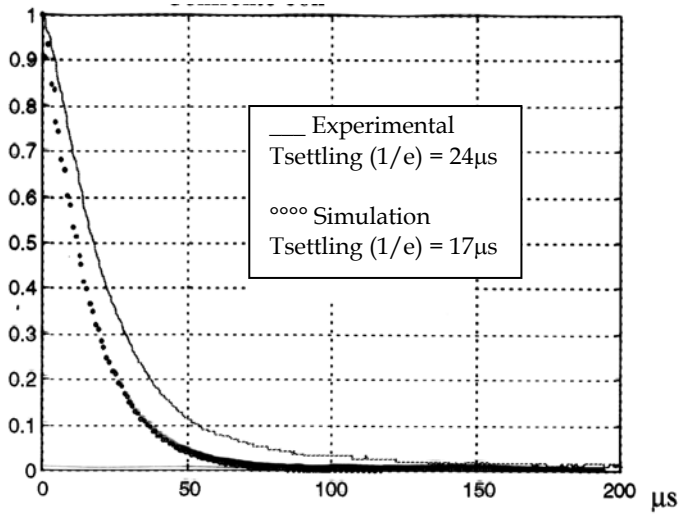

Fig. 7. Comparison of pyroelectric sensor normalized voltage response between simulated model and experimental sensor.

Several single-element detectors were built, which were able to follow laser pulses with rise time up to 0.003 ms. Figure 8 shows an example of the time response to a CO_2 laser pulse for the values reported in Table 2.

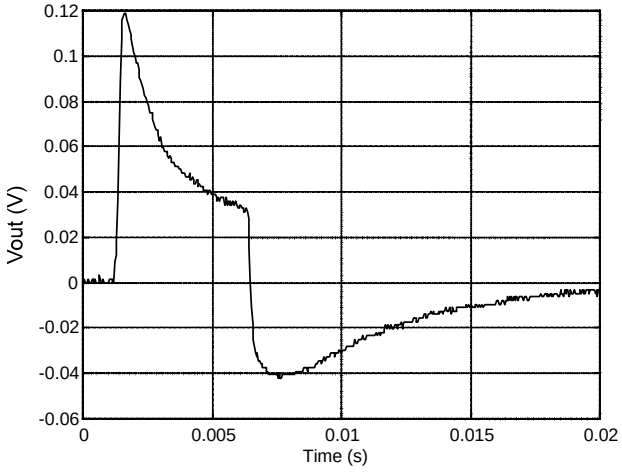

Fig. 8. Pyroelectric signal in response to a pulsed CO_2 laser

Active area of detector	9 mm^2
Thickness(PVDF)	40 μm
Gold metallisation	0.1 μm
Z_{el}	Ra= 1 MΩ parallel with Cc= 15 pF
Pulsed laser characteristics	
PRF	50 Hz
Duty cycle	22%

Table 2. Parameter values characterising detector and laser source for the measurement shown in Figure 8

The time response is characterized by a rising time 0.2 ms like that of the laser pulse and the undershot is characteristic of a rapid cut-off. The recovery time (7 ms at 1/e of Vout max) is governed by the detector thermal time constant $R_T C_T$.
The settling time to zero value is mainly determined by the undershoot and it is approximately 15 ms.
This basic example demonstrates the feasibility of the pyrolectric PVDF film sensor technology for monitoring IR laser pulses (Capineri et. al., 1992). Another technology that has been demonstrated useful for sensor fabrication availed of a screen printed pyroelectric paste (Capineri[b] et al., 2004). Both pyroelectric materials have been employed to design and build array of sensors with different configuration and size, depending on the application (Capineri et al. 1998)(Capineri et al., 2005)(Mazzoni et al.,2007). Some example of pyroelectric arrays used to design monitoring devices for CO_2 power laser systems are described in the following section.

3. Technologies for PVDF pyroelectric sensor arrays

Commercially available pyroelectric arrays mostly employ ferroelectric materials as BST, PbSe, $LiNbO_3$ and $LiTaO_3$. These sensors are fabricated with technologies which are compatible with integrated electronics. Their spatial resolution is determined by the pitch between elements, typically 50 μm wide for arrays in the order of 320x240 pixels. Their performances in terms of sensitivity and NEP are suitable for thermal imaging applications and for remote temperature measurements (Muralt, 1996)(Capineri[b], 2004). The aim of this section is to describe enabling technologies for the development of low-cost pyroelectric sensor arrays for the beam characterization of CO_2 power lasers (λ=10.6 μm). A low-cost pyroelectric material PVDF is commercially available in the form of thin foils that can be metalized by means of evaporation or sputtering. The polymer foils are mechanically flexible and necessitates of fabrication technologies suitable for realizing the electrical contacts; rigid carrier substrates and low temperature conductive epoxy are usually employed for this aim. In this section, we describe some solutions that exploit printed circuits boards technology. The array of sensors should sustain relatively high power densities even if a beam power partitioning system is considered. Experimental characterization of sensors with PVDF foils with gold metallization in different conditions of laser pulses (peak power, duty cycle and pulse repetition frequency), showed that an average power density of 1 W/cm^2 should not be exceeded. An array element pitch of 1 mm was estimated sufficient to detect most of the significant anomalies of the laser beam intensity spatial distribution of a CO_2, 40 W continuos power laser.

A fabrication technology that can be adopted for a fast production of small series of sensors is the laser ablation (Capineri[a] et al. , 2004). In the following we describe the main features of the laser microfabrication for patterning electrodes on the film, and the line connections routing strategy. Two examples are shown: a matrix array (8x8 elements, pitch 1.45 mm) and a linear array (10x1 elements, pitch 1 mm). Preliminary experimental results on laser microdrilling of the PVDF material will be presented for microvias fabrication aimed to make individual contacts of each front electrode element. For the packaging we adopted the bonding of the sensor array to printed circuit boards and standard connectors for the external contacts to the front-end electronics board.

3.1 Laser microfabrication for ferroelectric polymer (PVDF) sensors

Polymer ferroelectric materials like PVDF are now commercially available from several manufacturers and are used for fabricating pyroelectric and ultrasonic piezoelectric sensors (Binnie et al., 2000)(Ritter et al. 2001). The relative merit of polymers respect to ceramics is their low weigh, mechanical flexibility, non reactivity to chemical agents and relative low cost with respect to piezoelectric ceramics. On the contrary, they have a limited operating range (T_{MAX}=80°C) and generally a lower figure of merit with respect to other piezoelectric or pyroelectric materials (De Cicco et al., 1999). In our application the choice of PVDF was mandatory for the large area required to monitor the position and intensity spatial distribution of a laser spot of about 1 cm^2.

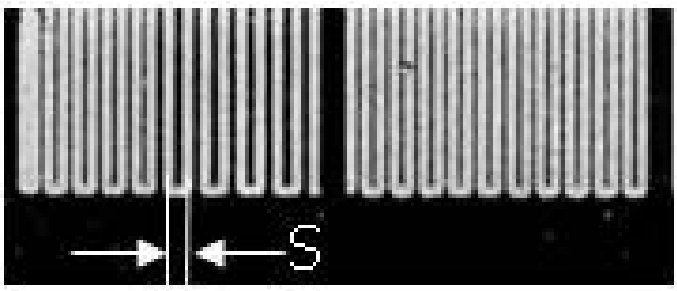

Fig. 9. Example of laser ablation of a set of parallel lines at two different separation distances S on a 40μm thick gold metallized PVDF film: (Left) S_1=150 μm , (Right) S_2=100 μm.

Considering the high incident power available, the sensor current responsivity requirements are not stringent and the transimpedance amplifiers can be designed with feedback impedances in the range 10MΩ-1GΩ; these values are not so large to be influenced by parasitic capacitances due to circuit layout or connection lines through the packaging. For the temporal diagnostics of the CO_2 laser pulses a response time better than 10 μs is needed.
The use of a plastic film as active pyroelectric material requires a suitable technology to transfer the design of the electrodes pattern on one or both sides of the film. The routing of electrical lines from the central elements of the matrix array to the external connector pins asked also for solutions adequate to the element miniaturization which needs line width negligible respect to the element size. In our approach we used a Nd:YAG laser (λ=1.064μm) marking tool (mod. Lasit, EL.EN. s.p.a., Italy) to ablate the metallizations of the PVDF film which are typically made with gold, aluminum, or even conductive silver ink, according to the optical and electrical requirements. The process has been developed for metallization

with thickness ranging from 0.1μm to 10μm which are typical of evaporation and screen-printing respectively. The laser ablation process needs to be optimized by successive refinements of the laser marking parameters such as the pulse repetition frequency, laser pumping current, pulse duration and focal distance. The laser setting was tuned according to the trace width (microfabrication features), the minimum induced mechanical film damage, the process repeatability and the electrodes design flexibility.
An interesting characteristic of the laser microfabrication is the contemporary ablation of the metallization on both sides of the film (Capineri[a] et al., 2004). After the ablation of the front electrodes metallization, the laser beam reaches the bottom side of the PVDF film without being absorbed by the bulk. This is possible due to the low absorption of the thin PVDF film at the Nd:YAG emission wavelength. In this way the patterning of the electrodes on both sides is attained with only one laser ablation run. The replica of the same pattern on both sides of the PVDF film is useful when differential connections to individual elements of the array are needed; differential transimpedance amplifiers can be employed for improving the common mode noise rejection as shown in Figure 6. The laser microfabrication method has been successfully demonstrated for different PVDF film thickness ranging from 9 μm to 110 μm.
In Figure 9 the results of a spatial resolution test is shown. The minimum distance S between two lines or two array elements should result higher than about S = 140 μm. In Figure 10, the zoom over a portion of the linear array reported in Figure 11(A) shows a detail of the gold metallized areas with rounded ablated corners.

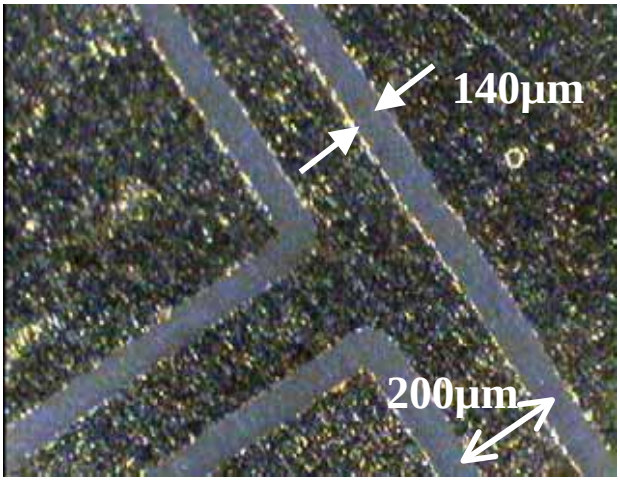

Fig. 10. Example of electrodes patterning by laser ablation.

Because of the low capability of this type of film to sustain overheating beyond 80°C, a study was performed to verify the presence of an eventual damage to the PVDF material. In particular, we compared the pyroelectric responses of single elements obtained by two different techniques, i.e. laser ablation and gold metal evaporation. No significant difference was observed. Some examples of fabricated pyroelectric arrays on 40 μm thick gold metallized PVDF film are reported in Figure 11 (A) and (B).
In Figure 11(A) the box indicates the active area of a linear array with 10x1 elements of dimensions 0.9x2mm^2 each, pitch 1 mm and connection lines width 0.2 mm. Four such

arrays were mounted at 90° angle on an electronic board in order to monitor the position and dimensions of a CO_2 laser beam in real-time. In Figure 11 (B) a fine pitch matrix array for beam spatial intensity distribution measurements is shown; it is provided with 8x8 elements, of area 1.25x1.25mm² and pitch 1.45 mm.

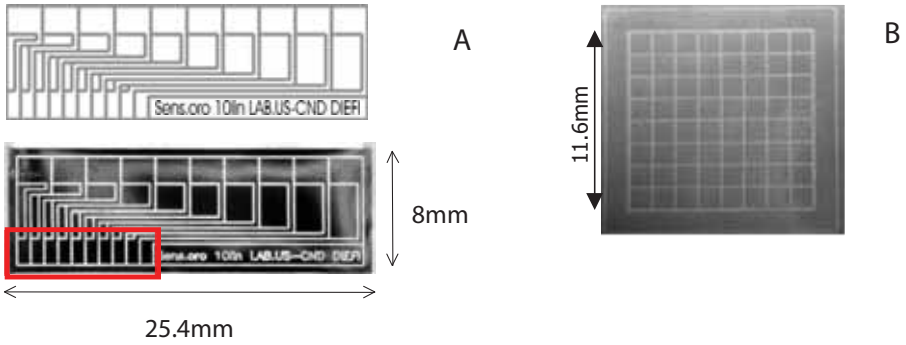

Fig. 11. A) AUTOCAD drawing for design the electrodes geometry of a linear array (top) and resulting sensor microfabrication (bottom). The rectangle in red color indicates the array of 10 active elements. B) matrix array: 8x8 square elements, side 1.25 mm, pitch 1.45mm.

The solution adopted for bonding the PVDF pyroelectric arrays to a rigid substrate utilizes two PCBs, called here top and bottom Printed Circuit Boards (PCB), called here top and bottom PCBs. The electrical connections between the film and PCBs are obtained by conductive epoxy (type EP21TDC/N, MasterBond, USA) and curing at room temperature. The PCBs have copper pads which overlap the gold pads on the PVDF film. This bonding technique proven to be reliable having used the sensors over a period of at least two years with no change in characteristics and performances. The routing from the external pads towards the active elements is not a problem for the linear array geometry.

On the contrary, the routing of the connection lines of the two-dimensional array poses the problem of individually contacting the front electrodes exposed to the radiation. Moreover, the connection line surface acts as a spurious sensor that creates cross-talk effects and ghost signals at the outputs of the sensor array. At present, our laser microfabrication technology with a Nd:Yag laser (not specifically devoted to this application) provides an ablated line width of 140 μm, which is the minimum pitch between matrix elements or conducting lines. Looking for novel solutions to this problem, we investigated a new structure for assembling matrix arrays that retains the advantages of the laser microfabrication and the packaging techniques previously described. We also developed a fabrication process for electrodes patterning on a PVDF film metallized only on one side. The opposite side was metallized in a second step by evaporating a single continuos semitransparent gold electrode of thickness less than 100 nm. This process provides a common front electrode for all elements which is connected to a top PCB and then to ground. The exposure of this front electrode to the incident beam occurs through a protection window (ZnSe or Ge) in the top PCB (see Figure 12). The front common electrode is grounded and the 64 single ended transimpedance amplifiers are connected by a standard PGA 84 pin connector.

The PVDF sensor was then bonded on the 64 central pads of the bottom PCB by using a programmable robot provided with a dispenser. This step of the fabrication is critical

because the uniformity and reliability of the bonding process can be easily affected by the conductive epoxy viscosity variability during the dispensing and curing phases. The sandwich of the two PCBs and sensor in between is then soldered to the PGA 84 pins connector. The photo in Figure 13 shows one prototype of the matrix pyroelectric array.

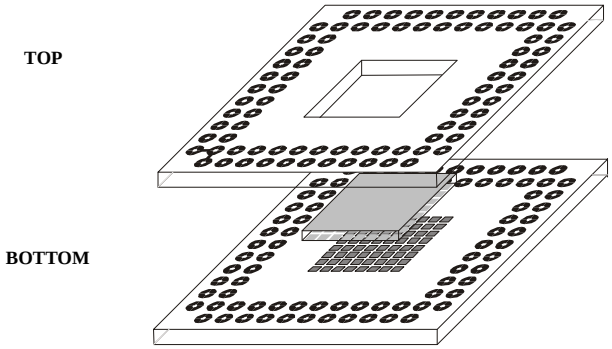

Fig. 12. Assembly for the pyroelectric matrix array.

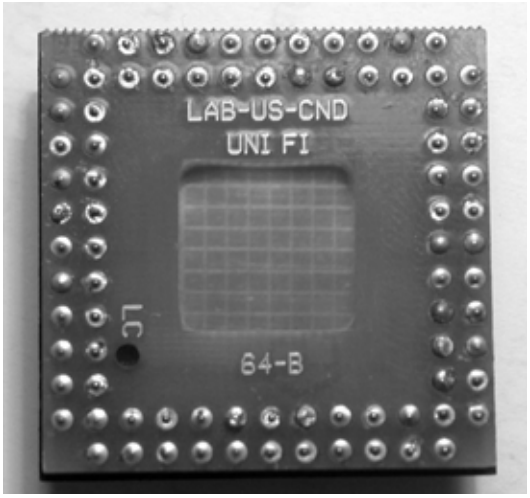

Fig. 13. Packaging for the pyroelectric matrix array.

The 64 elements matrix array have been characterized in terms of voltage responsivity and response uniformity. A thermal cross-talk ranging from -33dB to -41dB was found in the frequency range 10Hz-200Hz. The diagram in Figure 14 is an example of measured cross-talk on one element with side L=2.25 mm. It was obtained with a modulated laser diode at repetition frequency of 185 Hz and a laser spot diameter 500 μm. The results indicate that the lateral heat conduction of the front semi-transparent electrode is modest. We also found that it is slightly dependent on the beam modulation frequency. However, in the perspective of increasing the number of elements, the modification of the original design of the matrix array will consist of square elements in the front electrode contacted to a bottom PCB

through microvias. A reasonable value for the microvias diameter is in the range 10-50 μm, according to the minimized pitch of the array. Preliminary results of microdrilling with a duplicated Nd:YAG source have produced a line of through holes with diameters ranging from 20μm to 40μm (see Figure 15). The variation of the holes diameter is due to different settings during the laser process. Similar processing methods have been also explored more recently from other authors (Rabindra et al., 2008) (Lee et al., 2008).

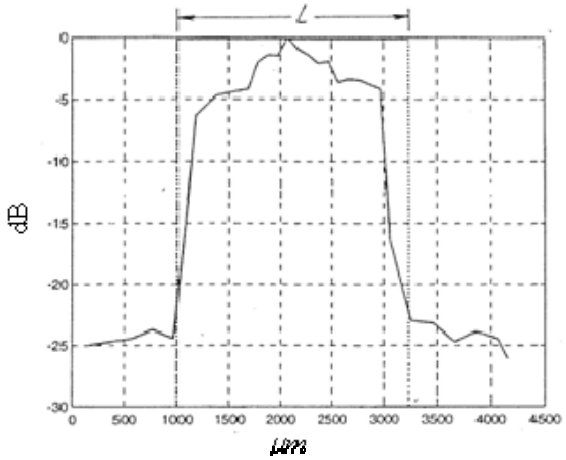

Fig. 14. Cross-talk measured on a single element at laser beam modulation frequency of 185 Hz.

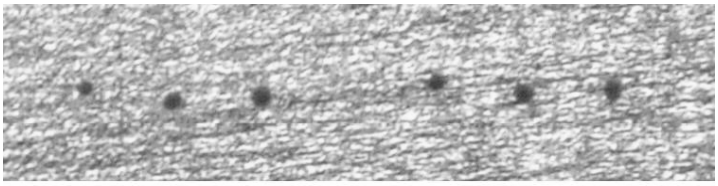

Fig. 15. Laser microdrilling through a 40 μm thick gold metallized PVDF film. The holes diameter varies from 20μm to 40μm.

4. Applications of PVDF pyroelectric array of sensors for CO_2 laser monitoring

In this section we explore the main applications of pyroelctric arrays in a linear and matrix configuration.

Pyroelectric sensor linear arrays of PVDF were found particularly suitable for the control of the spot dimensions of high power infrared laser beams. The sensors were tested for maximum power density in temporal cycles of tenths hours each.

We designed an optoelectronic instrument for the *on line* measure of the dimensions of the laser spot emitted by a multikilowatt CO_2 industrial laser. Due to the high power and long service time the optical components are subjected to thermal stresses which cause variation of the laser beam characteristics (shape and position).

In Figure 16 we show the schematic diagram of the experimental apparatus which consists of the laser source, a beam expander, a beam deflector and a focussing lens. The main beam of continuos power Pi is sampled after the beam expander by using a diffractive optics which splits the beam into a reflected beam, of power Pr=98.8% Pi, and a sampled beam of lower power and equal to 0.5% Pi. This low power beam of about 15 W (for a Pi=3 kW) has a typical diameter of 25 mm and follows the variations of the main one. We could measure its dimensions along two perpendicular directions with the linear array configuration shown in figure 17. The minimum required spatial resolution was 1mm and the variation of the dimensions were in the range of 20 mm – 30 mm.

We verified the damage threshold of the sensors made of gold metallized PVDF film with an experimental set-up in which the power density on the sensor was varied by changing the repetition frequency and duty cycle of an average power equal to 30 W which was delivered by the CO_2 laser source. A single sensor was irradiated through a metal diaphragm in cycles lasting tenths of hours each at increasing power density ranging from 0.15 W/cm^2 to 3 W/cm^2. The voltage response of the sensor was tested during each phase and the results are shown in Figure 18. The sensor response remained constant for a fixed value of the power density and it decreased for higher power density values owing to the increase of the sensor average temperature. At a value of 3.6 W/cm^2 we observed the destruction of the sensor, hence we safely reduced the power threshold value to 3 W/cm^2.

In Figure 19, we show an assembled linear array prototype; each of the four arrays is composed of ten elements with pitch 1 mm. Other measured characteristics of the fabricated linear array sensors are:

- Thermal cross-talk better than -40 dB at 200 Hz
- Bandwidth (-3dB): 257 Hz
- Current responsivity max: 190nA/W

The linear arrays in cross configuration have been experimented for real-time beam diameter monitoring but their use was extended also to laser power monitoring according to their useful bandwidth. It has been demonstrated that at fixed pulsed repetition frequency these sensors provide a reliable estimation of the incident laser power. Moreover, the fabrication technology explained in the previuos section, allowed the realization of pitches between elements of about 150 μm. This value is adequate also for real-time imaging of power laser beams by devising a rotating reflector that scanned the beam section at an angular velocity adequate for granting an accurate imaging of the laser pulse (Coutouly et al., 1999)(Akitt et al., 1992)(Mann et al., 2002), (Mazzoni et al., 2007).

4.1 Dual use of pyroelectric arrays for CO_2 and Nd:YAG laser pulses: laser pulse characterization and beam positioning

Industrial and medical CO_2 laser equipment are controlled for the optimization of the power emission according to the process. This normally implies two operation modes: continuous (CW) and pulsed (PW). In both cases it is important to monitor some beam parameters in real-time for maintaining the quality of the process or for diagnostic purposes (to check the functional anomalies). For both modes sensors are necessary that can operate at the laser wavelength (mid-IR) with an electronic instrument suitable for acquiring, processing and visualizing the beam parameters. The considered parameters were: the beam point stability, the beam spatial intensity distribution and the laser pulse shape related to the instantaneous emitted power. The measurements of these parameters are standardized (ISOFDIS

11146,11670,11554) and each one requires specific characteristic of the sensor and processing electronics. The pyroelectric array of sensors described in the previuos sections are suitable for these applications and represent a good compromise between cost and performances.

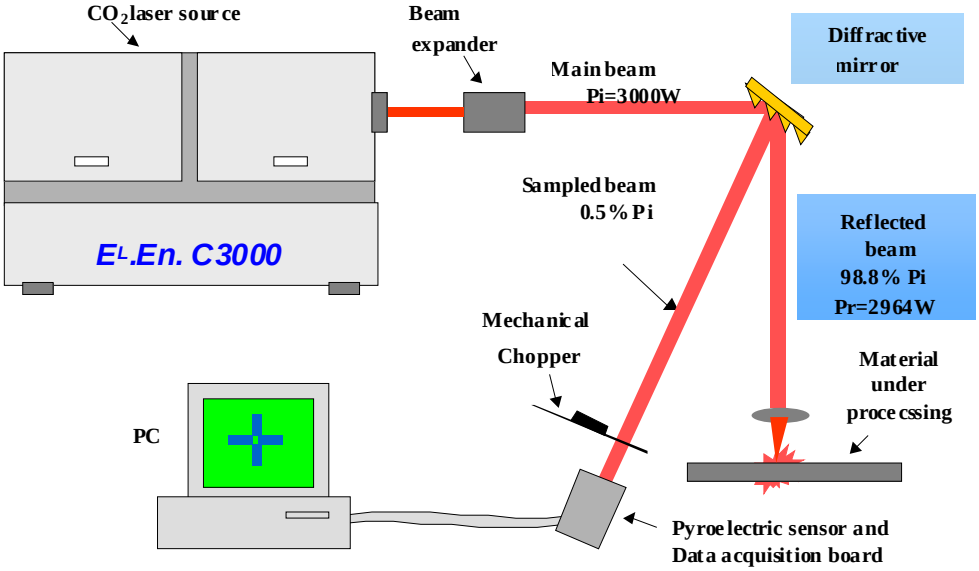

Fig. 16. Schematic diagram of diagnostic system of laser beam dimensions.

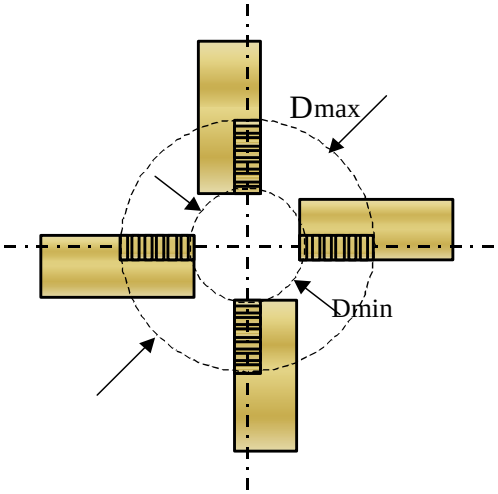

Fig. 17. Configuration of linear arrays for measuring the beam dimensions in the range Dmin-Dmax.

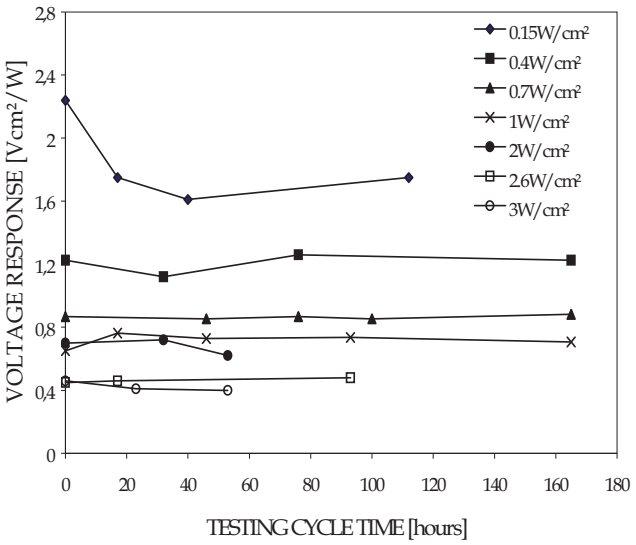

Fig. 18. Voltage response for different incident power densities during life tests.

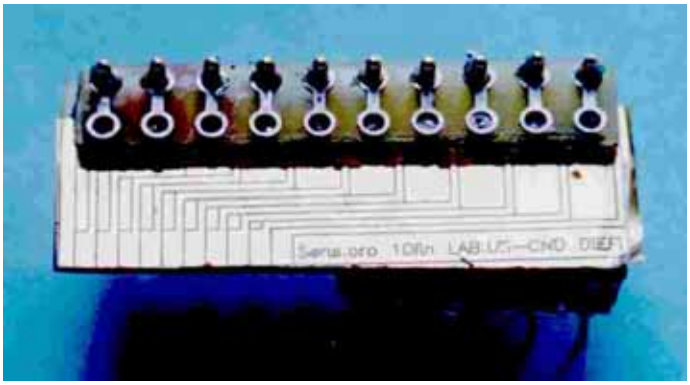

Fig. 19. Assembled linear array of 10x1 elements.

In this section it will be shown that a versatile instrument can be interfaced to different measuring modules provided with linear or matrix arrays of pyroelectric sensors. The two measuring modules were: Module "BeamScan64" for the laser spatial intensity characterization, and Module "PosIRix" for the laser beam point stability and pulse shape characterization (Capineri et al. 1999)(Capineri et al., 2005). The architecture can be replicated with other choices of the analog electronic components and with a microcontroller with upgraded performances.

4.2 Portable electronic instrument architecture

The instrument operates in a stand-alone mode and automatically switches the running program depending on the connected external module. The analog signals from up to 64 channels are digitally converted by two parallel ADCs on chip of a microcontroller Hitachi SH7044 and presented on a QVGA LCD with 256 colors. The instrument was tested with two sensor modules: an 8x8 matrix array for laser beam mapping with 64 high gain (1GΩ) transimpedance amplifiers, and a large area four-quadrant sensor for the beam point stability (Capineri et al. ,1999) control and laser pulse monitoring. The complete architecture of the analog-to-digital mother board is shown in Figure 20 and a photo of the prototype system is shown in Figure 22. The instrument is interfaced to external modules by a versatile bus (V-Bus) that includes several I/O digital lines, 64 analog lines, and several auxiliary lines for power supplies and remote sensing/controls. Inputs for an automatic identification of the plugged-in modules were also provided.

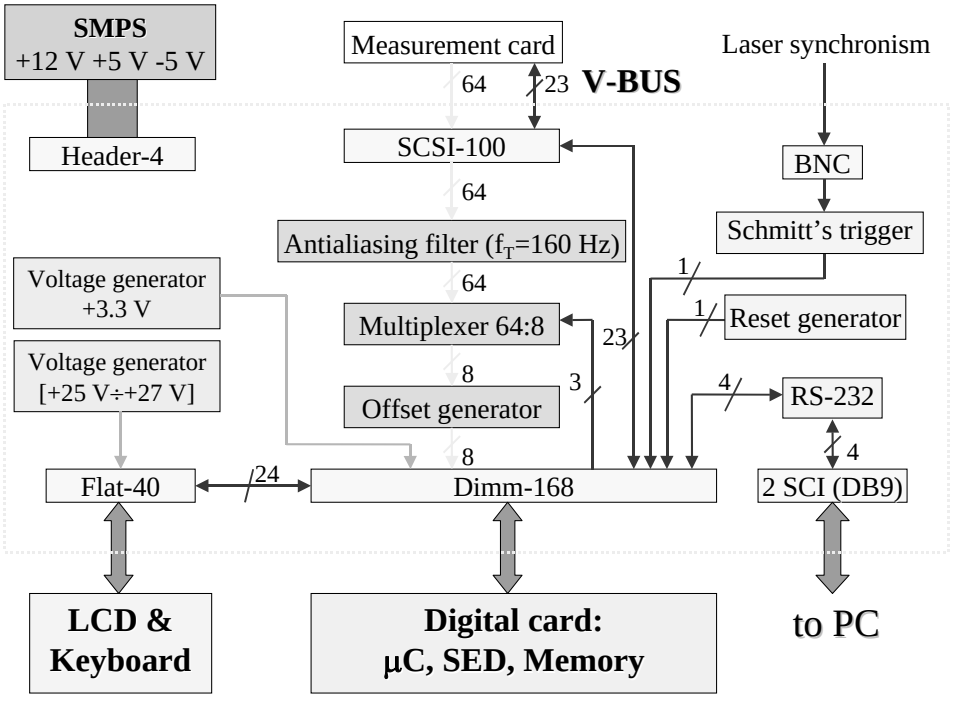

Fig. 20. Block scheme of the mother board of the electronic instrument

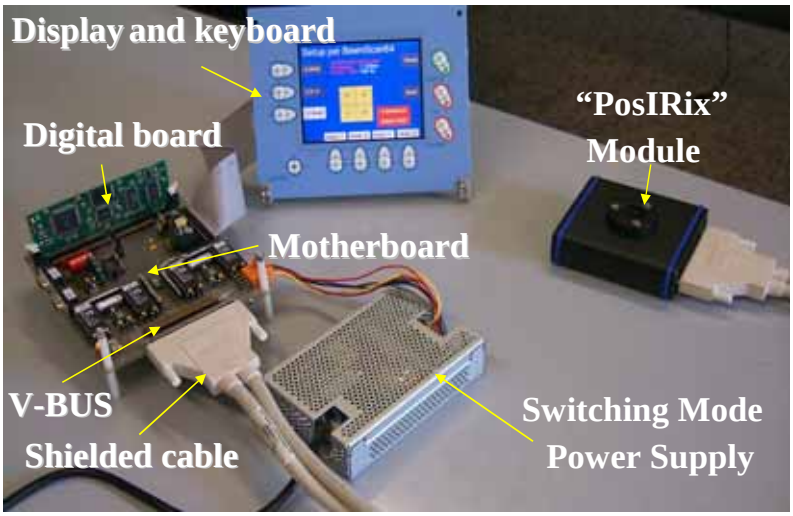

Fig. 21. Photograph of the components of the electronic instrument for IR laser beam characterisation

Fig. 22. Electronic board of the module PosIRix. In the bottom side, the DB5 type connector for the instrument V-Bus connection is sided in a central position; on the left side is shown the BNC connector for laser pulse monitoring by an oscilloscope. On the top left a 28mm x 28 mm PVDF four quadrant sensor with a circular ZnSe window for spectral filtering the CO_2 wavelength.

5. Module "PosIRix" for laser beam point stability and pulse shape characterization

This module consists of a 28 mm x 28 mm sensor divided in four quadrants by laser ablation of a gold metallized PVDF ferroelectric film of thickness equal to 40 μm. The pyroelectric material was bonded to a FR-4 epoxy rigid substrate with thermal conductive glue. The substrate was also used to make electrical contacts with bottom electrodes. The sensor fabrication was optimized in order to achieve the maximum sustainable power density D_{PMAX} and the maximum bandwidth of the voltage responsivity BW_{MAX}. This choice of the sensor design parameters (dimensions, substrate, bonding) is an example of good compromise among cost, bandwidth, sustainable power density and mechanical robustness. The sensor and front-end electronics were characterised with different powers, duty cycles and pulse repetition frequencies of a CO_2 laser source. Values of D_{PMAX} =2W/cm² and BW_{MAX} (-3dB) =18 kHz were found with a 4.4 MΩ transimpedance amplifier. We also demonstrated the adaptability of this sensor to a specific medical application of the laser by designing an electronic equalization filter of the amplitude of the frequency response in order to achieve a flat bandwidth (±1dB) between 10Hz and 18 kHz. In this way the laser pulse shape was reproduced with high fidelity, even for PRF as low as 10 Hz, in a range where the responsivity of the sensor is not flat. Two examples are reported in Figure 23 and 24. They show the reconstruction of the pulse shape of a CO_2 laser modulated at a PRF equal to 30 Hz and 100 Hz, respectively. In the same figures, we showed the response measured with a large bandwidth (20 MHz), small-size (i.e. 1mm²), commercial HgCdTe photovoltaic sensor for comparison.

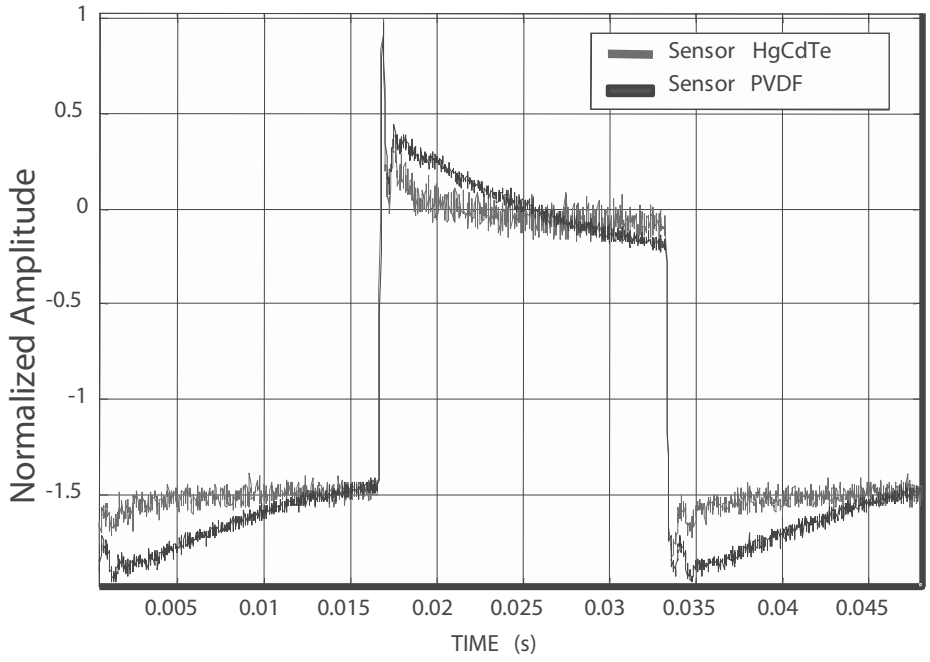

Fig. 23. CO_2 Laser pulse shape at PRF 30 Hz.

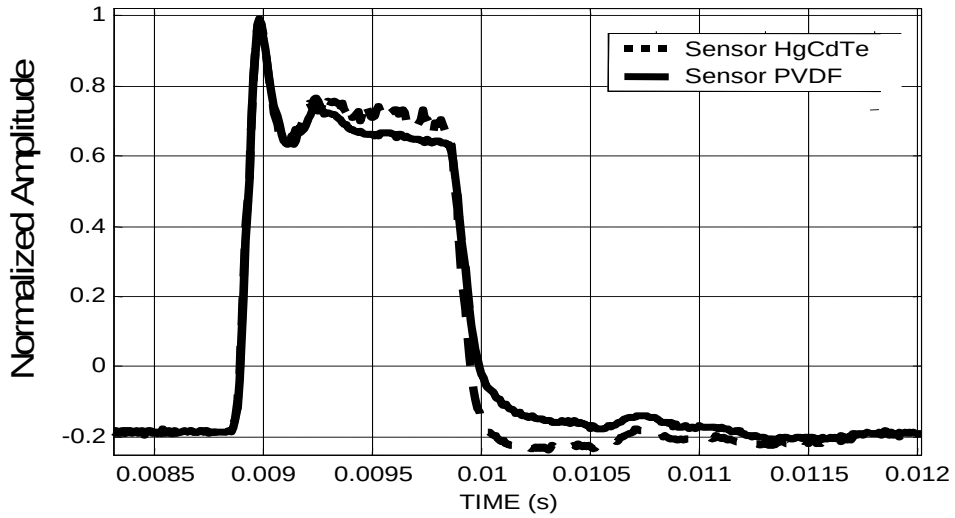

Fig. 24. CO_2 Laser pulse shape at PRF 100 Hz.

The same module was also used for monitoring the laser beam point stability by designing a programmable narrow band filter centered at the PRF of the laser source; this narrowband signal was digitized and fed to an algorithm that estimates the centroid of the intensity spatial distribution on the sensor plane (Capineri et al. 1999) with four quadrant signals. The algorithm is implemented on the microcontroller used in the portable instrument described in Section 4.2. The complete block scheme of this module is reported in Figure 25.

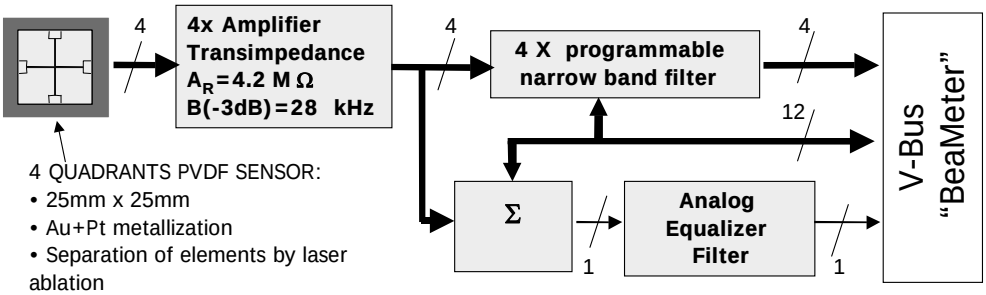

Fig. 25. Electronic analog signal processing carried out by module "PosIRix".

5.1 Signal filtering for limited bandwidth sensors

Two new implementations were developed for the processing and visualization of signals generated by PVDF pyroelectric sensor arrays with compensation filtering (Capineri et al. 2005) aimed to improve the reconstruction accuracy of CO_2 laser pulses. These implementations were especially devoted to biomedical applications for which there is a stringent demand for an accurate reproduction of both the fast and slow components of the laser pulse for the evaluation of the intensity in these two temporal regimes. The

implementations were realised for the module "Posirix" which was described in the previous section. It was primarily designed for laser beam positioning and allows the visulization of the laser pulse by an oscilloscope or by a dedicated instrument with real-time display. For the laser pulse envelope evaluation we used the sum of the signals from the four pixels to make the first temporal information independent of the beam centroid position within the sensor matrix array. For this solution, a requirement for achieving an accurate pulse reconstruction are four elements with the same frequency response.

5.2 Design of the analog filter

For the filter project of the bandwidth limited sensor we used the ideal compensation filter consisting in the classical inverse filter $H_c(f)$ defined as:

$$H_C(f) = \frac{K}{H(f)} \tag{3}$$

where K is a gain factor for a flat frequency response of the summing amplifier, and $H(f)$ is the sensor voltage frequency response. For the fitting function H_{fit} we used a bi-quadratic form in order to keep its realization simple by means of an analog filter. The fitting program was developed in Matlab (Mathworks, USA) and calculated the vector of coefficients a_i of the biquadratic function resulting from the minimization of the mean square error (*err*). This program required the following input parameters:

- a *vector* with the initial values of a_i;
- the frequency values *fmin* and *fmax* delimiting the range for the fitting of $H_{fit}(f)$ with $H_C(f)$;
- the vector with input data $H_c(f)$ interpolated in the range 1Hz – 50 kHz at 10 Hz steps.
- the tolerance on the functional value *(err)* and on the coefficient values a_i, the maximum number of iterations and of elaboration on *err*.

The *vector* with the initial a_i values was found with a trial procedure of few iterations using the minimization function "*fminsearch*" which starts from an initial guess of the coefficients and a rather high tolerance value to grant an uniform error density also in the frequency region with less data The program progressively decreases the tolerance value to increase the precision in the determination of the optimal vector of coefficients a_i.

The values *fmin* and *fmax* have been chosen to get a small ripple in the sensor bandwidth, particularly sensitive to the pole positions. After some trials they were set to 100 Hz and 7 kHz, respectively, so as it was impossible to cover the full range with only one biquadratic function. We had to use another filter function to complete the filter project.

For obtaining the complete transfer function of the compensation filter, we found the biquaquadratic coefficients for the following function,

$$H_{fit2}(f) = \frac{1}{H(f) \cdot H_{fit}(f)} \tag{4}$$

that we multiplied by the "high frequency" filter function $H_{fit}(f)$ to find the final filter function. By using the procedure described above to cover the remaining "low frequency" regions, the *fmin* and *fmax* values were set to 15 Hz and 250 Hz this time, with a superposition of the minimizing frequencies ranges of the two fitting functions of about 150 Hz. The final fitting function $H_{filt}(S=j2\pi f)$ resulted:

$$H_{filt}(S) = \frac{1,89S^4 + 48957S^3 + 2,16 \cdot 10^7 S^2 + 3,06 \cdot 10^9 S + 5,04}{S^4 + 3,82 \cdot 10^4 S^3 + 1,79 \cdot 10^7 S^2 + 1,89 \cdot 10^9 S + 3,25 \cdot 10^9}. \quad (5)$$

With H_{filt} the compensated filter bandwidth at –3dB extended from 4.4 Hz to 17.8 kHz with a ripple in band of 0.43 dB.
The function can be factorized into four terms which have a direct correspondence with the four building blocks A, B, C, D shown in Figure 26.
The analog design considered components values and tolerances commercially available, and it was started from a six order function H_{cf} with two nearly equal poles and zeroes that allowed more flexibility and no substantial filtering performance variation as shown in Figure 27.

5.3 Design of the digital filter

The digital filtering has the advantage of a circuit reduced dimension and uses the same analytical transfer function found for the analog implementation. Its capability is limited by the Hitachi SH2 microprocessor implementation on board of the same instrument. With a 128kByte RAM it is possible to use only numerical filter of the type IIR for their reduced computational request with respect to FIR ones. Furthermore, owing to the precision limitation to 32 bit of the microprocessor, the implementation of the transfer function resulting from the bilinear transformation of the sampled $H_{filt}(f)$ function at f_{sampl}=115.2 kHz requires an accurate analysis of the zeroes and poles position for the filter stability determination. We found that this implementation made the low frequency filtering worse and required the elimination of a zero-pole couple on the unitary circle corresponding to a frequency of about 10 Hz. We also evaluated the artefacts introduced in the transformation from the analog to the digital masks consisting in modulus and phase differences between the implemented and bilinearly transformed functions above 20 kHz as shown in Figure 28.
With a cascade of two filter cells of the second order, the execution time to perform the complete filtering of one laser pulse was about 7.59 μs, slightly less than the time between two samples ($1/f_{sampl}$ = 8.68 μs). Hence it was possible to perform the filtering in real time, and successively give a representation of the pulse envelope on a LCD display. Owing to the reduced dynamic of this monitor, the comparisons with the analog and digital filtering where performed on a PC, after acquisition of the signals from the sensor with an oscilloscope. The digital filter was realized with Matlab functions (Filter, qfilt), in this case.
Experimental results obtained with modulated CO_2 laser beams, at pulse repetition rates from 10 Hz to 1000 Hz and variable duty cycle, proved an accuracy in the laser pulses reconstruction that is not available in the commercial IR beam positioning sensors.
The analog implementation results much more noisy, but the digital implementation suffer for the imposed limitations that make the low frequency components reproduction worse.

6. Conclusions

In this chapter we described the capabilities of pyroelectric sensors built by means of low-cost hybrid technologies based on PVDF films for monitoring pulses of IR lasers. The technologies presented here can be used to design large area sensors for measuring the beam characteristics of pulsed CO_2 power lasers. Details and useful references are provided to build measuring modules both for the beam centroid positioning and the temporal monitoring of the laser pulses. Criterions for designing analog or digital compensation

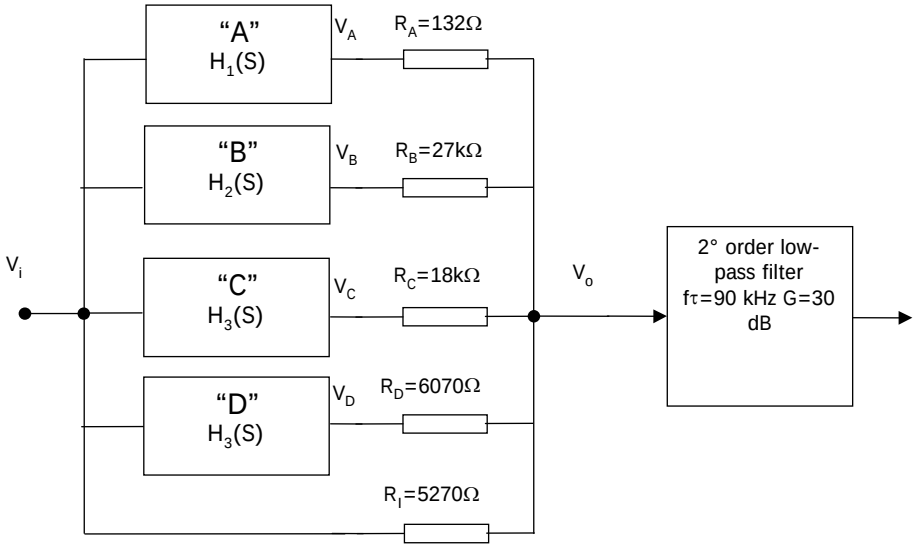

Fig. 26. (Top) Analog implementation of the filter function H_{filt} with four building blocks A, B, C, D. (Bottom) The Sallen-Key low-pass filter reduces the high frequency noise.

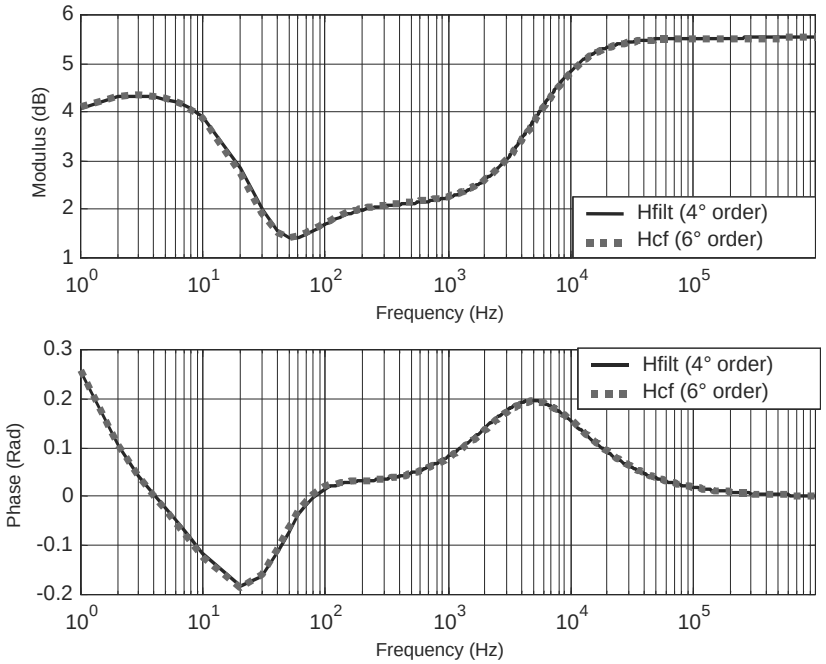

Fig. 27. Comparisons between computed fourth order H_{filt} and sixth order $H_c(f)$ implementations of the compensation filter function $H_c(f)$.

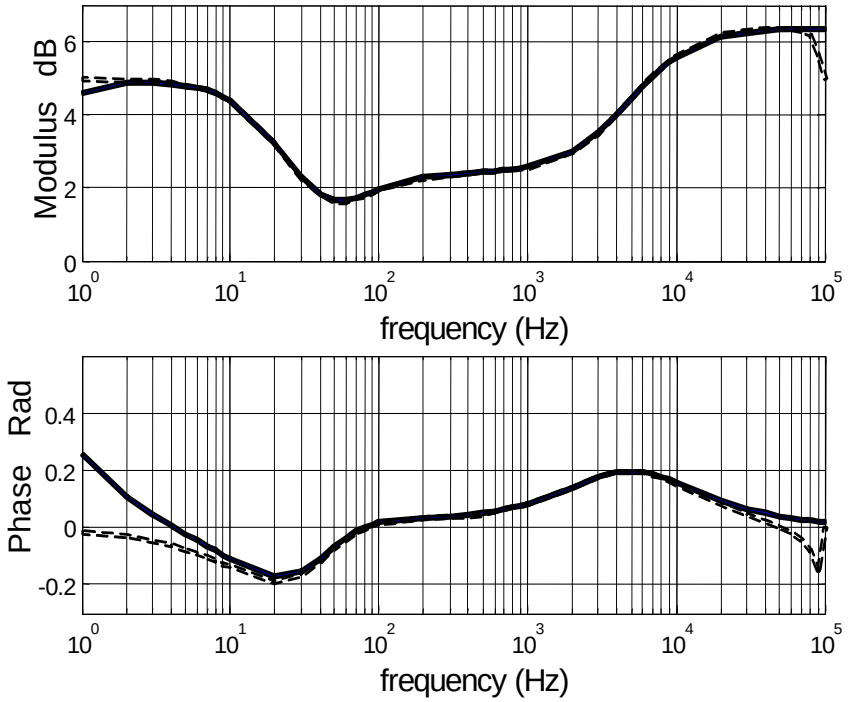

Fig. 28. Computed H_{filt} (continuos line) and numerical H_d (dashed line) implementations.

filters were provided in order to minimize the effect of the typical bandwidth of the pyroelectric thermal PVDF sensors. In this perspective the designed sensors can be seen as an external active probe of an oscilloscope and become an useful instrument for laboratories and companies where the IR laser sources are employed. The fabrication technology of PVDF pyroelectric arrays was reported and low-cost assembling and packaging solutions were presented. Future research for this type of sensors will deal with the analysis of a closed-loop control in real time of the laser system made now possible thanks to the computational power and versatility of commercially available microcontrollers.

7. Acknowledgments

The authors wish to acknowledge the support of CNR project MADESS II and Tuscany Region for having supported this project and the precious scientific and technical collaboration of Prof Leonardo Masotti (Università di Firenze, Italy), Dr Ing Giovanni Masotti (El.En. s.p.a.) and of all the master thesis students that made possible the realization of the projects.

8. References

Akitt D.R et al., (1992), Highperformance automatic alignment and power stabilization system for a multikilowatt CO_2 laser, *Rev. Sci. Instrum.*, vol. 63, pp.1859–1866, 1992.

Binnie T.D. et al., (2000) An integrated 16x16 PVDF pyroelectric sensor array, IEEE Transactions on UFFC, no. 47, pp 1413 –1420

Capineri L. et al. (1998), A 3x3 matrix of thick-film pyroelectric transducers, *Electronics Letters*, Vol. 34, pp 1486-1487

Capineri L. et al. (1999), A beam position sensor for low power infrared laser diodes, *Review of Scientific Instruments*, Vol. 70, pp. 1-8

Capineri L. et al., (2000), Pyroelectric PVDF sensor modeling of the temporal voltage response to arbitrarily modulated radiation, *IEEE Transactions on Ultrasonic and Frequency Control*, Vol. 47, pp. 1406-1412

Capineri[a] L. et al., (2004), European patent EP 1380821 "Matrix-type pyroelectric sensor, method for its fabrication and device for characterizing laser beams comprising said sensor "

Capineri[b] L. et al. (2004), Comparison between PZT and PVDF thick films technologies in the design of low-cost pyroelectric sensors, *Review of Scientific Instruments*, Vol. 75, , pp 4906-4910

Capineri L. et al. (2005), CO_2 laser pulse monitoring instrument based on PVDF pyroelectric array. *IEEE Sensors Journal*, Vol. 5, pp 520-529

Coutouly J.F. et al (1999), Simple is best for real-time beam analysis, *Opto Laser Europe*, n. 58, pp.34–37

De Cicco G. et al. (1999), Pyroelectricity of PZT-based thick-films, *Sensors and Actuators*, Vol. 76, pp. 409–415

Giacoletto L.J. & Landee R. W., (1977), *Electronics Designers Handbook* ed. McGraw-Hill, 0070231494, New York

Hammes P.C.A. & Regtien P.P.L., (1992), An integrated infrared sensor using the pyroelectric polymer PVDF, *Sensors and Actuators A*, Vol. 32, pp. 396-402

Kosterev A.A. et al. (2002), Chemical sensing with pulsed QC-DFB lasers operating at 15.6 μm, *Appl.Phys. B*, Vol. 75, pp.351-357

Lee S. et al. (2008), Femtosecond laser micromachining of polyvinylidene fluoride (PVDF) based piezo films, *Journal of Micromechanics and Microengineering*, Vol. 18, doi: 10.1088/0960-1317/18/4/045011

Mann S. et al., (2002), Automated beam monitoring and diagnosis for CO_2 lasers, Proceedings of SPIE 4629, Laser Resonators and Beam Control V, June 2002, pp. 112–121

Mazzoni M. et al., (2007), A large area PVDF pyroelectric sensor for CO_2 laser beam alignment, *IEEE Sensor Journal*, Vol. 7, pp. 1159-1164

Muralt P., (1996), Piezoelectric and pyroelectric microsystems based on ferroelectric thin films, *Proceedings of the Tenth IEEE International Symposium on Applications of Ferroelectrics*, Aug. 1996, pp. 145–151

Rabindra N. D. et al. (2008), Laser processing of materials: a new strategy toward materials design and fabrication for electronic packaging, *Circuit World*, Vol. 36 , ISSN: 0305-6120

Ritter T.A. et al. (2001), Development of high frequency medical ultrasound arrays, *2001 IEEE Ultrasonics Symposium*, August 2001, pp 1127 –1133

Rocchi S. et. al., (1992), A transducer modelling technique for the identification of the transfer function and driving-point impedance, *Sensors and Actuators A*, Vol. 32, pp. 361-365

Schopf H. et al., (1989), A 16-element linear pyroelectric array with NaNO2 thin films, *Infrared Physics*, Vol. 29, pp. 101-106

Setiadi D. & Regtien P.P.L., (1995), *Sensors and Actuators A*, Vol 46-47, pp. 408-412

Toci G. et al. (2000), Use of a PVDF pyroelectric sensor for beam mapping and profiling of a mid-infrared diode laser , *Rev. Sci. Instr.*, Vol. 71, pp. 1635 - 1637